

Signatures of regular black holes from the shadow of Sgr A* and M87*

Indrani Banerjee^{*1}, Subhadip Sau^{†2,3} and Soumitra SenGupta^{‡3}

¹Department of Physics and Astronomy, National Institute of Technology, Rourkela

²Department of Physics, Jhargram Raj College, Jhargram, West Bengal-721507

³School of Physical Sciences, Indian Association for the Cultivation of Science, Kolkata-700032

Abstract

With the recent release of the black hole image of Sgr A* alongside the earlier image of M87*, one can now really hope to acquire a better understanding of the gravitational physics at the horizon scale. In this paper, we investigate the prospect of the regular black hole scenario with a Minkowski core in explaining the observed shadow of M87* and Sgr A*. Regular black holes generally appear in Einstein gravity coupled to non-linear electrodynamics and are interesting as they can evade the $r = 0$ curvature singularity arising in general relativity. Using the previously determined mass and distance we compute the observables associated with the black hole shadow. These when compared with the observed angular diameter reveals that the shadow of M87* and Sgr A* favor the regular black hole scenario with a small but non-zero charge. The implications are discussed.

1 Introduction

Discovery of gravitational waves [1,2] and successful imaging of black holes by the Event Horizon Telescope collaboration [3–9] has opened up new avenues for testing general relativity (GR) in the strong field regime. This is important, since general relativity despite being the most successful theory in explaining gravitational interaction in all length scales has several shortcomings. In the observational side GR fails to adequately address the dark sector [10–13] while in the theoretical end, the theory is marred with unresolved issues like singularities [14–16]. Therefore, the need to understand the nature of strong gravity continues to be a subject of considerable importance.

Singularities are regions of spacetime where a theory loses its predictability and therefore it is believed that singularities should not exist in nature. However, the theorems proposed by Hawking and Penrose [17] state that singularities are inevitable in GR. It is often believed that a suitable theory of quantum gravity can resolve this issue and hence a number of quantum gravity models have been put forward [18–23]. An alternate route to address the singularity issue classically, is by studying black holes with a regular core [24–34]. For such black holes the curvature invariants are finite for all points in space time. These black holes have a horizon and the core at $r = 0$ is often of de Sitter or Minkowski type [35–40].

*banerjeein@nitrkl.ac.in

†subhadipsau2@gmail.com

‡tpssg@iacs.res.in

Regular black holes with a de Sitter core are more extensively studied [38–40]. This motivates us to study the less explored regular black holes with a Minkowski core. Such black holes arise in gravity theories coupled to non-linear electrodynamics where the source of Einstein’s equations correspond to an anisotropic fluid resembling Maxwell’s stress tensor far from the black hole [41]. As a result the metric resembles the Reissner Nörsdrom spacetime and the electric field assumes the form of the Coulomb field far from the source. Investigating the properties of such a black hole solution is important as the mass function is associated with an exponential convergence factor which makes the corresponding quantum gravity model finite to all orders [42]. A finite quantum gravity model is desirable as it can evade the cosmological constant problem [43] and avoid the divergences appearing in flat space quantum field theories.

Astrophysical black holes are generally rotating and since we wish to investigate the observational signatures of the aforesaid regular black hole, studying its rotating counterpart is important. Such a rotating solution is obtained by applying the Newman-Janis algorithm [44–47] to the static, spherically symmetric seed metric which has an exponential mass function. Just as the spherically symmetric solution resembles the Reissner Nörsdrom metric, the axisymmetric solution resembles the Kerr-Newman background far from the source [48].

The observational signatures of regular black holes have been studied quite extensively [49–61]. In this work we investigate the nature of the black hole shadow cast by the regular black holes discussed above. We derive the outline of the black hole shadow corresponding to the rotating solution which enables us to compute the observables like the angular diameter of the shadow, the deviation from circularity and the axis ratio. These are then compared with the observed image of M87* [3–9] and Sgr A* [62–67] which in turn enables us to establish novel constraints on the non-linear electrodynamics (NED) charge parameter of the two sources. Estimate of the NED charge parameter for some stellar mass black holes and Sgr A* has been done from observations related to quasi-periodic oscillations. The present analysis therefore opens up the opportunity to verify their mutual consistency.

The paper is organized in the following way: In Section 2 we briefly discuss the characteristics of the regular black hole solution with a Minkowski core arising in gravity coupled to non-linear electrodynamics. Section 3 is dedicated to deriving the outline of the black hole shadow for the regular spacetime studied in Section 2. In Section 4 we compare our theoretical results with the observed shadow of M87* and Sgr A* respectively, in particular, we compute observables like the shadow angular diameter, the deviation from circularity and the axis ratio which in turn enables us to conclude whether the regular black hole scenario is more favored compared to the Kerr scenario in GR. Finally we conclude with a summary of our results with some scope for future work in Section 5.

Here we work with mostly positive metric convention and assume $G = c = 1$ for our analysis.

2 Black hole in non-linear electrodynamics

The present work deals with regular black holes in non-linear electrodynamics with an asymptotically Minkowski core. The Lagrangian density associated with non-linear electrodynamics coupled to Einstein gravity is given by [24, 40, 49, 68–70],

$$S = \int d^4x \sqrt{-g} \left(\frac{\mathcal{R}}{16\pi} - \frac{L(F)}{4\pi} \right) \quad (1)$$

where \mathcal{R} denotes the Ricci scalar and $L(F)$ is the non-linear electrodynamics Lagrangian density. In Eq. (1) $F = F^{ab}F_{ab}/4$ corresponds to the Faraday invariant while $F_{ab} = \partial_a A_b - \partial_b A_a$ is the electromagnetic field

strength tensor with A_i the gauge field. In the weak field limit $L(F) = F$ and the Maxwell theory is retrieved. By varying the action with respect to A_i we obtain its corresponding equation of motion,

$$\{L_F F^{ij}\}_{;i} = 0 \quad (*F^{ij})_{;i} = 0 \quad (2)$$

where $L_F = \frac{\partial L}{\partial F}$ and $*F^{ij} = \epsilon^{ijkl} F_{kl}$ is the Hodge-dual of F^{ab} . On the other hand, variation of the action with respect to the metric leads to the Einstein's equations with $L(F)$ as the source,

$$G_{ab} = 2(L_F F_a^s F_{bs} - g_{ab}L(F)) \quad (3)$$

The first regular black hole solution was proposed by Bardeen [71] which eventually led to extensive work in this direction [25, 27, 30, 72–79]. Later Ayon-Beato and Garcia confirmed that the physical source associated with the Bardeen solution corresponds to the gravitational field of a nonlinear magnetic monopole of a self-gravitating magnetic field [24]. In general, the static and spherically symmetric solution of Eq. (3) assumes the form [49],

$$ds^2 = -\left(1 - \frac{2\hat{m}(r)}{r}\right) dt^2 + \left(1 - \frac{2\hat{m}(r)}{r}\right)^{-1} dr^2 + r^2 d\theta^2 + r^2 \sin^2\theta d\phi^2 \quad (4)$$

where the form of the mass function $\hat{m}(r)$ is determined by the properties of the non-linear electrodynamics source $L(F)$. For a spherically symmetric spacetime the non-zero components of the field strength tensor F_{ab} correspond to F_{tr} and $F_{\theta\phi}$. In the event the black hole carries a pure magnetic charge g the gauge field potential corresponds to $A = -g \cos\theta d\phi$ such that the only non-vanishing component of the field strength tensor is $F_{\theta\phi} = g \sin\theta$.

The Lagrangian density associated with non-linear electrodynamics leading to regular black holes with a monopole charge has the general form [49],

$$L(F) = \frac{\mu \mathcal{M}}{g^3} \frac{(2g^2 F)^{\frac{\nu+3}{4}}}{\{1 + (2g^2 F)^{\frac{\nu}{4}}\}^{1+\frac{\mu}{\nu}}} \quad (5)$$

Using the above Lagrangian density in Eq. (3), we obtain the following form of the mass function,

$$\hat{m}(r) = \frac{\mathcal{M} r^\mu}{(r^\nu + g^\nu)^{\mu/\nu}} \quad (6)$$

where \mathcal{M} is the black hole mass while μ and ν are positive, dimensionless constants appropriately chosen to ensure asymptotic flatness. It is important to note that the Schwarzschild solution is regained when μ vanishes. The mass function in Eq. (6) gives rise to a repulsive de Sitter central core for $\mu \geq 3$ and these two constants (μ and ν) can be suitably chosen to give rise to exact spherically symmetric regular black hole solutions. For example, $\mu = 3$ and $\nu = 2$ gives rise to the well-known Bardeen black hole solution while $\mu = \nu = 3$ leads to the Hayward black hole solution.

The black holes discussed so far are endowed with an asymptotically de Sitter core whereas in this work we are interested in regular black holes with an asymptotically Minkowski core. Such black holes have been proposed by Ayon-Beato and Garcia with mass function [25],

$$\hat{m}(r) = \frac{\mathcal{M} r^3}{(r^2 + q^2)^{\frac{3}{2}}} - \frac{q^2 r^3}{2(r^2 + q^2)^2} \quad (7)$$

and Lagrangian density,

$$L(F) = P \frac{(1 - 8\sqrt{-2q^2P} - 6q^2P)}{(1 + \sqrt{-2q^2P})^4} - \frac{3}{4q^2s} \frac{(-2q^2P)^{\frac{5}{4}}(3 - 2\sqrt{-2q^2P})}{(1 + \sqrt{-2q^2P})^{\frac{7}{2}}} \quad (8)$$

where q is the electric charge of the black hole, $s = \frac{|q|}{2\mathcal{M}}$ and $P = L_F^2 F$. The same authors also proposed another class of regular black hole with an asymptotically Minkowski core [80]. Such black holes are associated with the mass function,

$$\hat{m}(r) = \mathcal{M} \left\{ 1 - \tanh \left(\frac{q^2}{2\mathcal{M}r} \right) \right\} \quad (9)$$

which is obtained by solving Eq. (3) with the Lagrangian density,

$$L = 2PH_P - H \quad (10)$$

where,

$$H = P \{ 1 - \tanh^2(s\sqrt{-2q^2P}) \} \quad (11)$$

and $H_P = \frac{\partial H}{\partial P}$.

In the present work the Lagrangian density corresponding to non-linear electrodynamics is given by [49],

$$L(F) = F e^{-\alpha(2g^2F)^{1/4}} \quad (12)$$

such that $\alpha = g/(2\mathcal{M})$ with g being the magnetic charge and \mathcal{M} the mass of the black hole.

With the Lagrangian density in Eq. (12), the static, spherically symmetric and asymptotically flat solution of Eq. (3) assumes the form,

$$ds^2 = - \left(1 - \frac{2\mathcal{M}e^{-\kappa/r}}{r} \right) c^2 dt^2 + \frac{dr^2}{\left(1 - \frac{2\mathcal{M}e^{-\kappa/r}}{r} \right)} + r^2 (d\theta^2 + \sin^2\theta d\phi^2) \quad (13)$$

where $\kappa = g^2/2\mathcal{M}$.

Such a black hole solution arises as a result of solving Einstein's equations with the source [81],

$$\begin{aligned} T_0^0 &= -\rho(r) = \frac{-\mathcal{M}k}{4\pi r^4} e^{-k/r}; \\ T_1^1 &= -\rho(r) = \frac{-\mathcal{M}k}{4\pi r^4} e^{-k/r}; \\ T_2^2 &= T_3^3 = \frac{\mathcal{M}k}{4\pi r^4} \left(1 - \frac{k}{2r} \right) e^{-k/r} \end{aligned} \quad (14)$$

where $k = \kappa/r_g$ is the dimensionless magnetic monopole charge parameter with $r_g = GM/c^2$ the gravitational radius. It is interesting to note that the above energy momentum tensor is regular at $r = 0$ and vanishes as $r \rightarrow \infty$. Moreover, Eq. (14) is in accordance with the weak energy condition and reduces to the Maxwell stress tensor far from the horizon.

Since astrophysical black holes are in general rotating, studying the axisymmetric counterpart of Eq. (13) is observationally more relevant. The stationary, axisymmetric and asymptotically flat black hole solution of Einstein's equations with source given by Eq. (14) is obtained by applying the Newman-Janis algorithm [44–47] to the seed metric Eq. (13) [48]. The corresponding line element has been studied in [48, 49] and assumes the form,

$$ds^2 = -\left(1 - \frac{2\hat{m}(r)r}{\Sigma}\right)dt^2 - \frac{4a\hat{m}(r)r}{\Sigma}\sin^2\theta dt d\phi + \frac{\Sigma}{\Delta}dr^2 + \Sigma d\theta^2 + \left(r^2 + a^2 + \frac{2\hat{m}(r)ra^2}{\Sigma}\sin^2\theta\right)\sin^2\theta d\phi^2 \quad (15)$$

where,

$$\Sigma = r^2 + a^2 \cos^2\theta, \quad \Delta = r^2 + a^2 - 2\hat{m}(r)r \quad (16)$$

and a is the Kerr parameter. The mass function $\hat{m}(r)$ is given by,

$$\hat{m}(r) = \mathcal{M}e^{-\kappa/r} \quad (17)$$

such that $\lim_{r \rightarrow \infty} \hat{m}(r) = \mathcal{M}$. In Eq. (17) $\kappa = \frac{g^2}{2\mathcal{M}}$ has dimensions of length. Since it is computationally easier to handle dimensionless quantities we scale κ and r in Eq. (17) by the gravitational radius $r_g = GM/c^2$. Thus the dimensionless metric parameters correspond to the squared charge to mass ratio $k = \kappa/r_g = \frac{g^2 c^4}{2G^2 \mathcal{M}^2}$ and the spin parameter $a \equiv a/r_g$.

It is important to note that when $r \gg k$ the above metric reduces to the Kerr-Newman spacetime. In the absence of nonlinear electrodynamics $k = 0$ and Eq. (15) reduces to the Kerr metric. We further note that Eq. (15) has no curvature singularity at $r = 0$ but assumes an asymptotically Minkowski core, i.e. the energy density $\rho(r) \rightarrow 0$ as $r \rightarrow 0$ unlike a de-Sitter core where the energy density becomes constant at the core. Interestingly, the curvature invariants in the above spacetime can be described by the Lambert W function and exhibits several physically intriguing features [81–88].

In order to derive the horizon radii one solves for the roots of $g^{rr} = \Delta = 0$ which yields,

$$r^2 + a^2 - 2re^{-k/r} = 0 \quad (18)$$

For the metric in Eq. (15) to represent a black hole the horizons must be real and positive. This requirement sets the physically allowed range of k to $0 \lesssim k \lesssim 0.7$. In the next section we discuss the procedure to derive the outline of the shadow for the regular spacetime given in Eq. (15).

3 Shadow of regular black holes with Minkowski core

The boundary of the shadow bears the signatures of strong gravitational lensing of nearby radiation and therefore the nature of the shadow can potentially unravel valuable information regarding the characteristics of strong gravity near the black hole [89–93]. In this section we derive the nature of the black hole shadow for black holes discussed in Section 2 [94, 95]. Given a stationary, axisymmetric metric, the Lagrangian $\tilde{\mathcal{L}}$ for test particle motion is given by,

$$g_{\mu\nu}\dot{x}^\mu\dot{x}^\nu = g_{tt}\dot{t}^2 + 2g_{t\phi}\dot{t}\dot{\phi} + g_{\phi\phi}\dot{\phi}^2 + g_{rr}\dot{r}^2 + g_{\theta\theta}\dot{\theta}^2 = 2\tilde{\mathcal{L}} \quad (19)$$

The Lagrangian is equal to unity for massive particles and zero for massless particles. The corresponding Hamiltonian is given by,

$$\mathcal{H} = p_\mu \dot{x}^\mu - \tilde{\mathcal{L}} = \frac{1}{2} g^{\mu\nu} p_\mu p_\nu = \frac{k}{2} \quad (20)$$

with k the rest mass of the test particle which in the present context is zero. We use the Hamilton-Jacobi approach such that the Hamiltonian is related to the action S by,

$$\mathcal{H}(x^\mu, p^\mu) + \frac{\partial S}{\partial \lambda} = 0 \quad \text{where} \quad p_\mu = \frac{\partial S}{\partial x^\mu} \quad (21)$$

Since the metric in Eq. (19) is independent of t and ϕ , the specific energy \mathcal{E} and specific angular momentum \mathcal{L} are conserved quantities. These are given by,

$$\begin{aligned} \mathcal{E} = -p_t = g_{tt}\dot{t} + g_{t\phi}\dot{\phi} &= \text{constant} \\ \mathcal{L} = p_\phi = g_{\phi t}\dot{t} + g_{\phi\phi}\dot{\phi} &= \text{constant} \end{aligned} \quad (22)$$

From the above condition the action can be written as,

$$S = -\mathcal{E}t + \mathcal{L}\phi + S(r, \theta) \quad (23)$$

It turns out that for the metric in Eq. (15), Eq. (23) is separable such that, $S(r, \theta) = S^r(r) + S^\theta(\theta)$. Substituting Eq. (23) in equation Eq. (20) we get,

$$g^{rr} \left(\frac{dS}{dr} \right)^2 + g^{\theta\theta} \left(\frac{dS}{d\theta} \right)^2 + g^{tt} \mathcal{E}^2 - 2^{t\phi} \mathcal{E} \mathcal{L} + g^{\phi\phi} \mathcal{L}^2 = 0 \quad (24)$$

For the metric in Eq. (15) the above equation assumes the form,

$$\Delta \left(\frac{dS^r}{dr} \right)^2 + \left(\frac{dS^\theta}{d\theta} \right)^2 - \left\{ \frac{1}{\Delta} (r^2 + a^2)^2 - a^2 \sin^2 \theta \right\} \mathcal{E}^2 + \frac{4ar\hat{m}(r)}{\Delta} \mathcal{E} \mathcal{L} + \mathcal{L}^2 \left(\frac{1}{\sin^2 \theta} - \frac{a^2}{\Delta} \right) = 0 \quad (25)$$

Interestingly, the r and θ parts of the above equation can be separated such that,

$$\Delta \left(\frac{dS^r}{dr} \right)^2 - \frac{1}{\Delta} (r^2 + a^2)^2 \mathcal{E}^2 + \frac{4ar\hat{m}(r)}{\Delta} \mathcal{E} \mathcal{L} - \frac{a^2}{\Delta} \mathcal{L}^2 = - \left(\frac{dS^\theta}{d\theta} \right)^2 - a^2 \mathcal{E}^2 \sin^2 \theta - \frac{\mathcal{L}^2}{\sin^2 \theta} = C \quad (26)$$

where C corresponds to the Carter constant. The left hand of Eq. (26) depends only on r while the right hand side is a function of θ alone. The radial part of Eq. (26) can be written as,

$$\left(\frac{dS^r}{dr} \right)^2 = \frac{R(r)}{\Delta^2} \quad (27)$$

where

$$R(r) = \Delta[-C - (\mathcal{L} - a\mathcal{E})^2] - \{(r^2 + a^2)\mathcal{E} - a\mathcal{L}\}^2 \quad (28)$$

while the angular part can be written as,

$$\left(\frac{dS^\theta}{d\theta}\right)^2 = \Theta(\theta) \quad (29)$$

where,

$$\Theta(\theta) = C + \cos^2\theta \left(a^2 \mathcal{E}^2 - \frac{\mathcal{L}^2}{\sin^2\theta} \right) \quad (30)$$

The action therefore assumes the form,

$$S = -\mathcal{E}t + \mathcal{L}\phi + \int \frac{\sqrt{R(r)}}{\Delta} dr + \int \sqrt{\Theta(\theta)} d\theta \quad (31)$$

From Eq. (21), Eq. (27) and Eq. (29) we obtain the equations of motion for r and θ ,

$$\dot{r} = \frac{\sqrt{R(r)}}{\Sigma} \quad \text{and} \quad \dot{\theta} = \frac{\sqrt{\Theta(\theta)}}{\Sigma} \quad (32)$$

Estimates of the shape and size of the shadow are associated with the geodesic motion of photons in the black hole background. Since photons are charge neutral we have considered accretion of neutral test particles in the preceding discussion. It is however important to note that accretion of charged particles will have an impact on observables associated with black holes. In particular, when we are studying models to describe the continuum spectrum or quasiperiodic oscillations we are dealing with accretion of ions and electrons which are charged massive particles. In the event the black hole is also charged (as in the present case) the equations of motion get substantially modified due to the interaction of the charged particles with the electromagnetic field of the black hole [96,97]. This leads to a modification in the theoretical spectrum from the accretion disk and the epicyclic frequencies associated with the quasi-periodic oscillations [96,97]. Since photons are uncharged they do not directly interact with the electromagnetic field of the black hole. However, the charge of the black hole modifies the background metric compared to the Kerr scenario which in turn affects the motion of the photons. In other words the electromagnetic field of the black hole affects the motion of the photons through a change in the background spacetime only.

In order to proceed further we define two impact parameters,

$$\chi = \frac{C}{E^2} \quad \text{and} \quad \eta = \frac{L}{E} \quad (33)$$

From Eq. (32) one can show that the physically allowed region for the photon can never reach upto $\theta = 0$. The maximum allowed value of θ denoted by θ_{max} is given by,

$$\cos^2 \theta_{max} = \frac{-(\chi + \eta^2 - a^2) \pm \sqrt{(\chi + \eta^2 - a^2)^2 + 4a^2\chi}}{2a^2} \quad (34)$$

where χ can be positive, negative or zero.

3.1 Solving the radial equation

The differential equation associated with the radial part is given by,

$$\left(\frac{\Sigma}{E}\right)^2 \dot{r}^2 = \Delta \left[-\chi - \left(\frac{L}{E} - a\right)^2 \right] + (r^2 + a^2 - a\eta)^2 = V(r) \quad (35)$$

For spherical photon orbits one needs to satisfy the condition: $V(r) = V'(r) = 0$. The first condition gives:

$$\Delta(\chi + \eta^2 + a^2 - 2a\eta) = (r^2 + a^2 - a\eta)^2 \quad (36)$$

while the second condition leads to,

$$\chi + \eta^2 + a^2 - 2a\eta = \frac{2}{1 - \frac{\hat{m}(r)}{r} - \hat{m}'(r)} (r^2 + a^2 - a\eta) \quad (37)$$

Solving Eq. (36) and Eq. (37) we get two sets of solutions for η and χ parametrized in terms of r [94,95,98],

1.

$$\chi = -\frac{r^4}{a^2} \quad (38)$$

$$\eta = \frac{a^2 + r^2}{a} \quad (39)$$

2.

$$\chi = -\frac{r^3 (4a^2 r \hat{m}'(r) - 4a^2 \hat{m}(r) + r^3 \hat{m}'(r)^2 + 2r^3 \hat{m}'(r) - 6r^2 \hat{m}(r) \hat{m}'(r) - 6r^2 \hat{m}(r) + 9r \hat{m}(r)^2 + r^3)}{a^2 (r \hat{m}'(r) + \hat{m}(r) - r)^2} \quad (40)$$

$$\eta = \frac{a^2 r \hat{m}'(r) + a^2 \hat{m}(r) + a^2 r + r^3 \hat{m}'(r) - 3r^2 \hat{m}(r) + r^3}{a (r \hat{m}'(r) + \hat{m}(r) - r)} \quad (41)$$

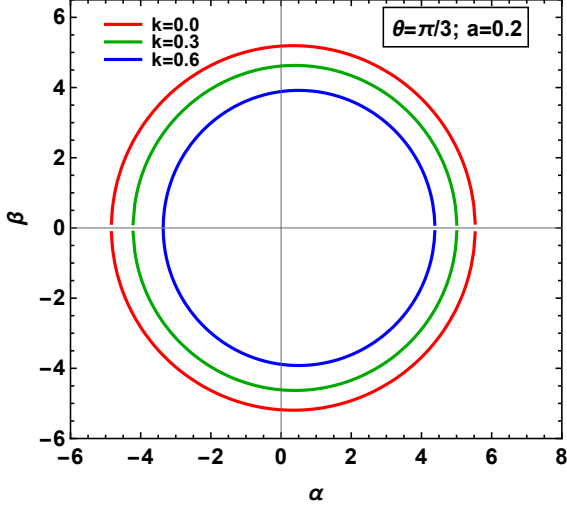
The first solution is not allowed physically [94,95,98] since this leads to $\Theta(\theta) < 0$ which is forbidden (see Eq. (32)). For the second solution χ may take either sign depending upon the value of r and accordingly the appropriate conditions need to be satisfied.

3.2 Deriving the shape of the black hole shadow

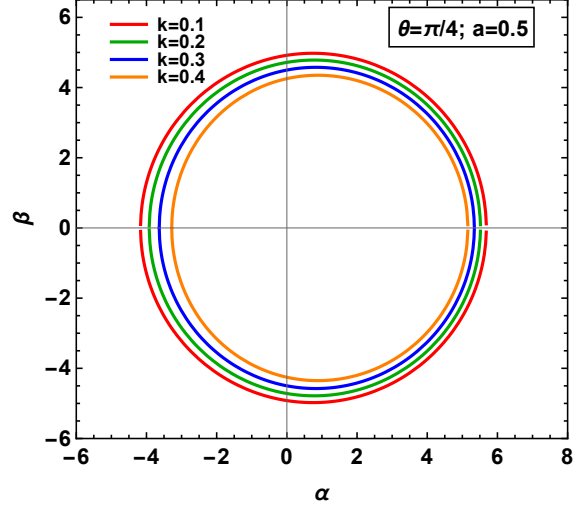
Deriving the impact parameters is important as they can be used to calculate the celestial coordinates $x = \alpha$ and $y = \beta$ of the black hole shadow as seen a distant observer at position (r_0, θ_0) . The apparent perpendicular distance of the image from the axis of symmetry is associated with the x coordinate while the apparent perpendicular distance of the image from the equatorial plane is associated with the y coordinate of the shadow.

To derive this we need to consider the Bardeen tetrads [99–102] which are associated with observers to whom the black hole appears non-rotating. These tetrads are given by,

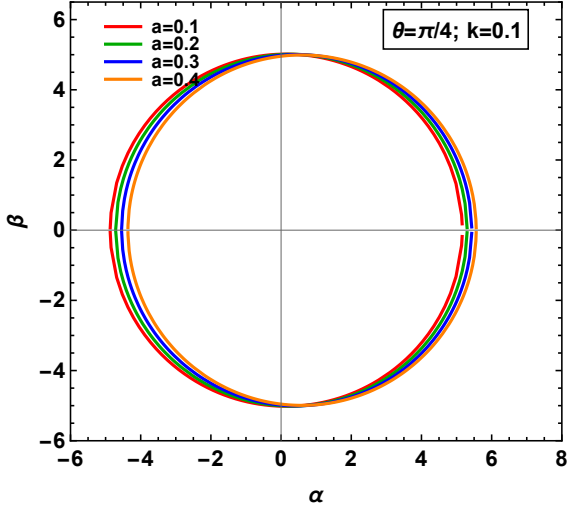
$$e_{(t)} = \sqrt{g^{tt}} \partial_t + \frac{g^{t\phi}}{\sqrt{g^{tt}}} \partial_\phi \quad (42)$$



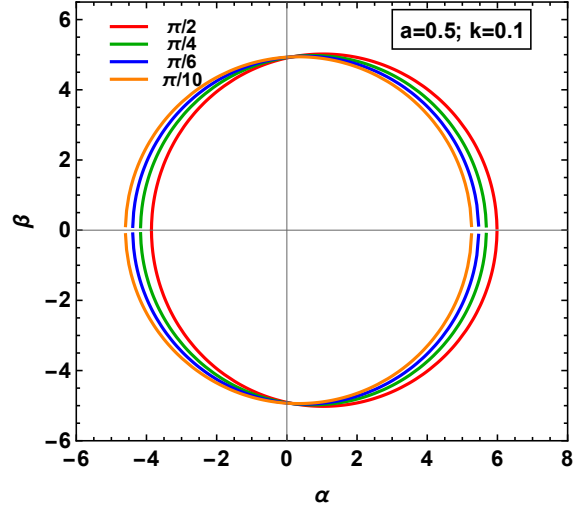
(a) Variation of BH shadow with metric parameter k . Here the inclination angle is taken to be $\theta = 60^\circ$ and the spin is assumed to be $a = 0.2$.



(b) Variation of BH shadow with metric parameter k . Here the inclination angle is taken to be $\theta = 45^\circ$ and the spin is assumed to be $a = 0.5$.



(c) Variation of BH shadow with spin-parameter a . Here the inclination angle is taken to be $\theta = 45^\circ$ and $k = 0.1$.



(d) Variation of BH shadow with inclination angle θ . Here the spin is taken to be $a = 0.5$ and $k = 0.1$.

Figure 1: Variation of the shape and size of the BH shadow with charge parameter k , spin parameter a and inclination angle θ . We note that with increase in θ and a the shadow becomes increasingly more dented.

$$e_{(r)} = \sqrt{|g^{rr}|} \partial_r \quad (43)$$

$$e_{(\theta)} = \sqrt{|g^{\theta\theta}|} \partial_{\theta} \quad (44)$$

$$e_{(\phi)} = \sqrt{|g^{\phi\phi}| + \frac{(g^{t\phi})^2}{g^{tt}}} \partial_{\phi} \quad (45)$$

The components of four momentum $p_{(a)}$ of a locally inertial observer are $p_{(a)} = e_{(a)}^j p_j$ while $p^{(a)} = \eta^{(a)(b)} p_{(b)}$ such that,

$$p^{(t)} = \frac{E}{c} \left(c\sqrt{g^{tt}} - \eta \frac{g^{t\phi}}{\sqrt{g^{tt}}} \right) \quad (46)$$

$$p^{(r)} = \pm \sqrt{\frac{R}{\Sigma\Delta}} \quad (47)$$

$$p^{(\theta)} = \pm \sqrt{\frac{\Theta}{\Sigma}} \quad (48)$$

$$p^{(\phi)} = \sqrt{|g^{\phi\phi}| + \frac{(g^{t\phi})^2}{g^{tt}}} \eta \quad (49)$$

Let $v_{(\theta)} = p^{(\theta)}/p^{(r)}$ and $v_{(\phi)} = p^{(\phi)}/p^{(r)}$ be the local apparent velocities of a given photon and r_0 and θ_0 the Boyer-Lindquist coordinates of the observer. In that event the apparent perpendicular distance from the axis of rotation and the equatorial plane are respectively given by $d_{\phi} = r_0 v_{(\phi)}$ and $d_{\theta} = r_0 v_{(\theta)}$. Since $\dot{\theta} \rightarrow 0$ and $\dot{\phi} \rightarrow 0$ for $r \rightarrow \infty$ the x and y coordinates of the shadow are respectively given by,

$$\begin{aligned} \alpha &= \lim_{r_0 \rightarrow \infty} \frac{r_0 p^{(\phi)}(r_0, \theta_0)}{p^{(r)}(r_0, \theta_0)} = -\frac{\eta}{\sin\theta_0} \\ \beta &= \lim_{r_0 \rightarrow \infty} \frac{r_0 p^{(\theta)}(r_0, \theta_0)}{p^{(r)}(r_0, \theta_0)} = \pm c\sqrt{\Theta(\theta_0)} \end{aligned} \quad (50)$$

In [Fig. 1](#) we plot the variation of the shape and size of the black hole shadow with change in the inclination angle θ , spin a and for various choices of the non-linear electrodynamics charge parameter k . Similar study has been done in [\[77, 103–105\]](#). From the figure it is evident that an increase in a and θ makes the shadow more deviated from the circular shape. Further, an increase in k decreases the size of the shadow.

4 Contact with observations

To find the effects beyond general relativity, we need to define observables associated with black hole shadow. The curve $\beta(\alpha)$ defines the boundary of the shadow. It is customary, for non-circular shadow structure, to define two axes (one major axis and one minor axis) corresponding to two diameters as shown in the [Fig. 2](#). The major axis is given by $\Delta\beta = \beta_t - \beta_b$, where β_t and β_b are respectively the topmost and the bottommost points of the shadow in the $\alpha - \beta$ plane. In a similar way, the minor axis is defined by $\Delta\alpha = \alpha_r - \alpha_l$, where α_r and α_l are respectively the rightmost and the leftmost points of the shadow. One can note that the shadow structure is symmetric upon reflection about the minor axis. Further the two axes i.e $\Delta\beta$ and $\Delta\alpha$ can also be expressed as a function of metric parameters and the inclination angle. Therefore, observables used to distinguish the shadow of a black hole in modified gravity to that of the

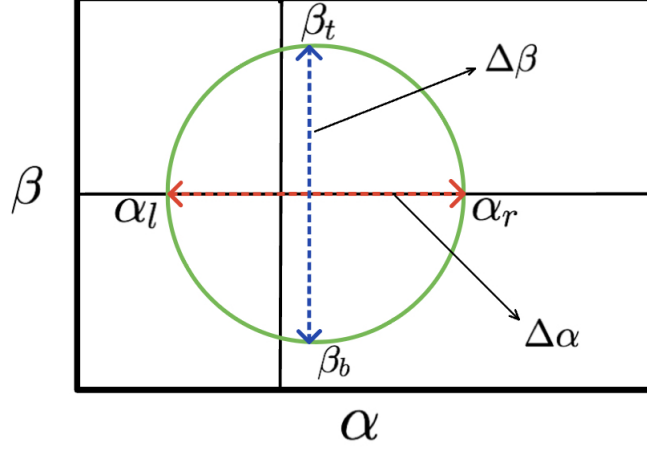


Figure 2: Major axis and minor axis of shadow structure

Kerr scenario in general relativity are:

(i) Angular diameter which is given by:

$$\Phi = \frac{GM\Delta\beta}{c^2D} \quad (51)$$

where M is the mass and D is the distance from the observer.

(ii) The axis ratio which is denoted by:

$$\Delta A = \frac{\Delta\beta}{\Delta\alpha} \quad (52)$$

(iii) Deviation from circularity ΔC : Unlike shadow of spherically symmetric metric, the shadow structure for Kerr-like solution looks like a deformed circle and hence it is important to define the observable, deviation from circularity. For this we first define the geometrical centre of the shadow which can be evaluated as $\alpha_c = \int \alpha dS / \int dS$ and $\beta_c = 0$ (due to reflection symmetry around minor axis), where dS is the area element. The distance between the geometrical centre and any point (α, β) on the shadow curve with azimuthal angle ϕ can be given by $\ell(\phi) = \sqrt{\{\alpha(\phi) - \alpha_c\}^2 + \beta^2(\phi)}$. Now one can define the deviation from circularity as follows

$$\Delta C = \frac{1}{R_{\text{avg}}} \sqrt{\frac{1}{2\pi} \int_0^{2\pi} d\phi \{\ell(\phi) - R_{\text{avg}}\}^2} \quad (53)$$

where, the average radius R_{avg} is defined as,

$$R_{\text{avg}} = \sqrt{\frac{1}{2\pi} \int_0^{2\pi} d\phi \ell^2(\phi)} \quad (54)$$

4.1 Constrains on the non-linear electrodynamics charge from the shadow of M87*

In this section we compare our theoretical findings with the observed shadow of M87*. As reported by the Event Horizon Telescope (EHT) collaboration, the supermassive black hole M87* at the centre of the galaxy M87 has the following observational parameters [4, 8, 9]:

1. Angular Diameter: $42 \pm 3 \mu as$ [4, 8, 9].
2. Deviation from circularity: $\Delta C \lesssim 10\%$ [4, 8, 9].
3. Axis ratio: $\lesssim 4/3$ [4, 8, 9].

The mass of the source has been measured previously by investigating the motion of stars and gas clouds moving very close to the black hole. From stellar dynamics measurement the mass of the source is $M \simeq 6.2_{-0.5}^{+1.1} \times 10^9 M_\odot$ [106], while study of gas dynamics reveals that the mass of M87* is $M \simeq 3.5_{-0.3}^{+0.9} \times 10^9 M_\odot$ [107]. The distance of the source has been estimated from stellar population measurements which turns out to be $D = (16.8 \pm 0.8)$ Mpc [108–110]. Based on the angle the jet axis makes to the line of sight and assuming that the axis of rotation coincides with the jet axis, the inclination angle is estimated to be 17° [4, 8, 9]. Further, from the measurement of the angular diameter of the shadow, the EHT collaboration reports the mass of the source to be $M = (6.5 \pm 0.7) \times 10^9 M_\odot$.

It is important to note that in order to evaluate the angular diameter theoretically one needs to provide the mass and the distance (Eq. (51)) while the dependence on the background metric is encapsulated in $\Delta\beta$. In Fig. 3 and Fig. 4 we plot contours of angular diameter of M87* as a function of a and k . In both the figures the angular diameter is evaluated based on the previously measured distance $D = 16.8$ Mpc. In Fig. 3a the angular diameter is calculated assuming $M \sim 6.2 \times 10^9 M_\odot$ while the angular diameter in Fig. 3b assumes $M \sim 3.5 \times 10^9 M_\odot$. For completeness we report the angular diameter as function of a and k assuming $M = 6.5 \times 10^9 M_\odot$ in Fig. 4 (which is the mass derived from the shadow itself).

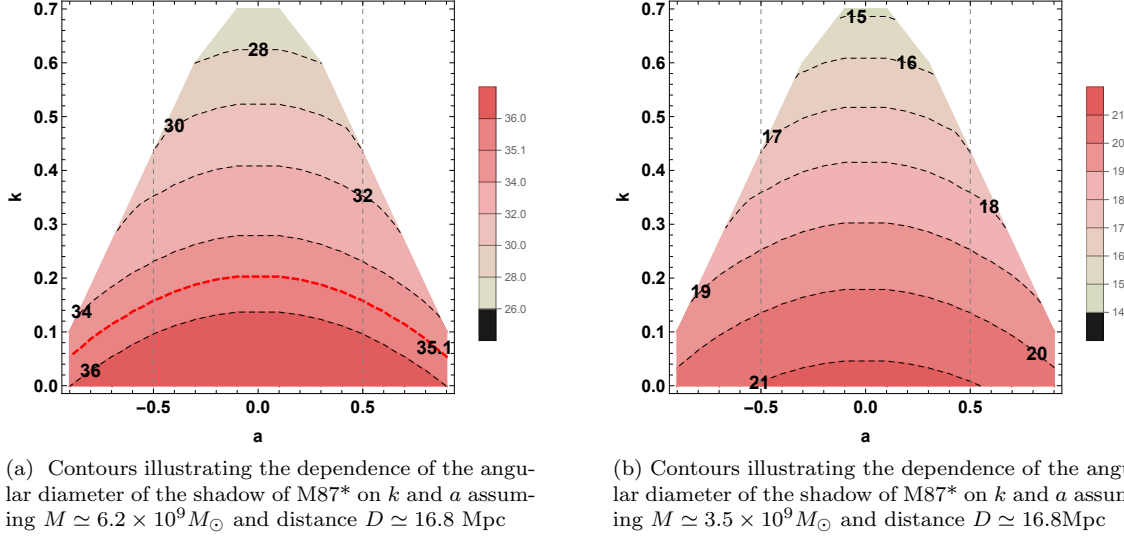


Figure 3: The above figure depicts the angular diameter of the shadow of M87* in the (k, a) plane assuming the previously determined mass and distance.

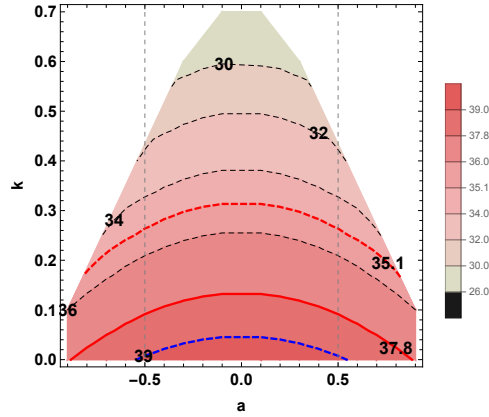
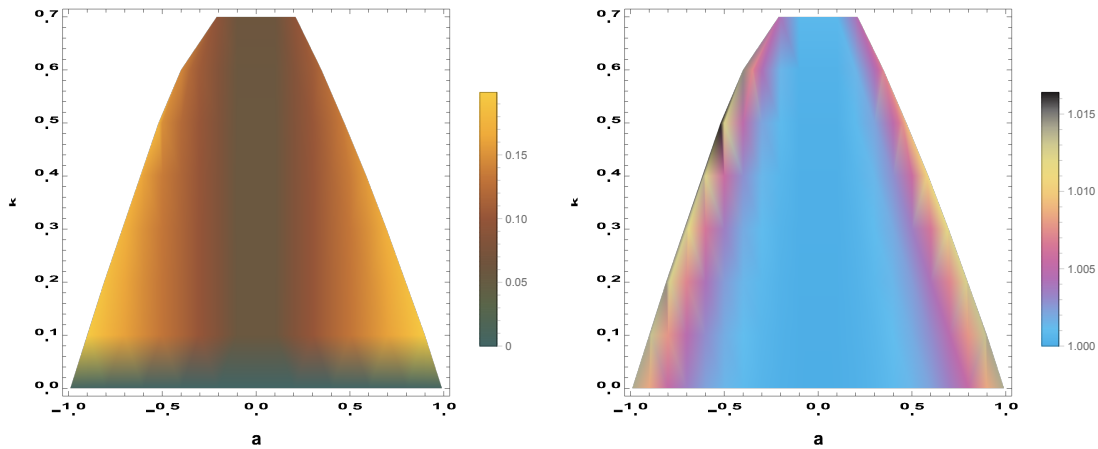


Figure 4: In the figure above we plot the angular diameter of the shadow of M87* in the (k, a) plane assuming distance $D \simeq 16.8$ Mpc and mass $M \simeq 6.5 \times 10^9 M_\odot$ (which is the mass estimated from the shadow itself).

At this point it is important to recall that the measured angular diameter of the shadow is $42 \pm 3 \mu\text{as}$. However, there is a 10% offset between the image diameter and the shadow diameter, i.e the true shadow can be at most as small as $37.8 \pm 2.7 \mu\text{as}$. Therefore, it is clear from Fig. 3b that $M \simeq 3.5 \times 10^9 M_\odot$ cannot reproduce the observed angular diameter of the shadow. It is clear from Eq. (51) that angular diameter



(a) The above figure shows the variation of ΔC with k and a assuming an inclination angle of 17° corresponding to M87*.

(b) The above figure shows the variation of ΔC with k and a assuming an inclination angle of 17° corresponding to M87*.

Figure 5: In the figure above we plot the variation of ΔC and ΔA as function of k and a . The inclination angle is taken to be 17° to obtain the plots.

is directly proportional to the black hole mass. Thus one might expect that a higher value of mass should reproduce the observed angular diameter. However, it is clear from Fig. 3a that when $M \sim 6.2 \times 10^9 M_\odot$ is taken, even the central value corresponding to the maximum 10% offset ($37.8 \mu\text{as}$) cannot be reproduced. This might probably be the reason why the mass of M87* reported by the EHT Collaboration is greater than the previous estimates. We will discuss more on this towards the end of this section. From the rejection table of [8] the spin values that can best explain the observations correspond to $|a| = 0.5$ and $|a| = 0.94$. Thus when $M \sim 6.2 \times 10^9 M_\odot$ is used, a small value of k ($0.05 \lesssim k \lesssim 0.15$) barely reproduces the angular diameter of the shadow within $1 - \sigma$ confidence interval, if we assume the maximum 10% offset $(37.8 - 2.7) \mu\text{as} = 35.1 \mu\text{as}$. This is depicted by the red dashed line in Fig. 3a. From Fig. 1 it is evident that an increase in k shrinks the shadow diameter and therefore the above discussion elucidates that the Kerr scenario or a small value of k can better explain the observed angular diameter of M87*.

Since an increase in mass increases the theoretical angular diameter of the shadow (Eq. (51)), when $M \simeq 6.5 \times 10^9 M_\odot$ is assumed and $|a| > 0.5$ is taken, $0 \lesssim k \lesssim 0.1$ can reproduce the centroid value of the shadow angular diameter with 10% offset. This is marked with red solid line in Fig. 4. With this mass even a very small k can reproduce the image diameter within $1 - \sigma$ ($39 \mu\text{as}$, marked with blue dashed line in Fig. 4). However, $M \simeq 6.5 \times 10^9 M_\odot$ should not be used to deduce the preferred value of k from shadow related observations as this mass is itself derived from the shadow diameter.

It is important to note that the data related to deviation from circularity ΔC can establish independent constraints on the magnitude of k (Fig. 5a). Since $\Delta C \lesssim 0.1$, for low spin values, nearly all allowed values of k seem to be favored by observations. However, the spin values that can best explain the observed jet power correspond to $|a| = 0.5$ and $|a| = 0.94$ (from the rejection table of [8]). For $|a| \gtrsim 0.5$ the values of k that satisfy $\Delta C \lesssim 0.1$ constrain correspond to $0 \lesssim k \lesssim 0.1$ which is consistent with our conclusion from the observation related to angular diameter. Finally from Fig. 5b we note that the third observable, i.e.

axis ratio $\Delta\beta/\Delta\alpha \lesssim 4/3$ cannot provide any further constrain on the magnitude of k [4] as the maximum axis ratio realized in our case is 1.02.

4.2 Constrains on the non-linear electrodynamics charge from the shadow of Sgr A*

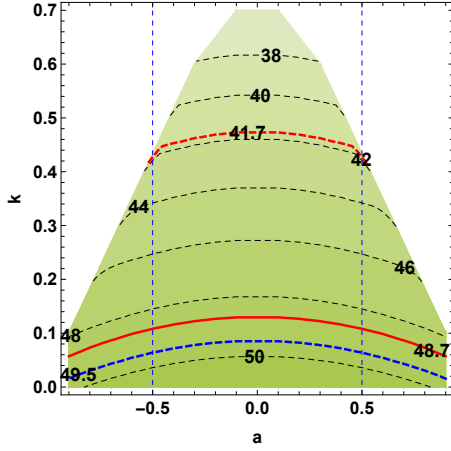
The recently observed shadow of Sgr A* can be used to establish constrains on the non-linear electrodynamics charge parameter, in the event the galactic centre black hole is considered to be a regular black hole with a Minkowski core. The mass and distance of the black hole is well constrained by several groups. Estimates on distance and mass measurements by the Keck team reports $D = 7959 \pm 59 \pm 32$ pc and $M = (3.975 \pm 0.058 \pm 0.026) \times 10^6 M_\odot$ (for fits that leave the redshift parameter free). Assuming the redshift parameter to be unity, the distance and mass measurements by the Keck team yield $D = 7935 \pm 50$ pc and $M = (3.951 \pm 0.047) \times 10^6 M_\odot$ respectively. The Gravity Collaboration estimates the distance and mass of Sgr A* to be $D = 8246.7 \pm 9.3$ pc and $M = (4.261 \pm 0.012) \times 10^6 M_\odot$ respectively. By taking into account the systematics due to optical aberrations the GRAVITY collaboration constrains the mass and distance of Sgr A* to $M = 4.297 \pm 0.012 \pm 0.040 \times 10^6 M_\odot$ and $D = 8277 \pm 9 \pm 33$ pc respectively.

The Event Horizon Telescope reports that the angular diameter of the emission ring of Sgr A* is $51.8 \pm 2.3 \mu\text{as}$ while the shadow angular diameter is $48.7 \pm 7 \mu\text{as}$. By comparing the observed image of Sgr A* with models based on extensive numerical simulations, one concludes that the inclination angle of the source is $i < 50^\circ$. In order to obtain the theoretical angular diameter of Sgr A* we need to use a specific value of the inclination angle. In this work we consider $i \simeq 134^\circ$ (or equivalently 46°) [111]. We keep k and a variable and derive the angular diameter as a function of k and a using the aforesaid inclination angle and the various combinations of mass and distance discussed above. This is illustrated in Fig. 6.

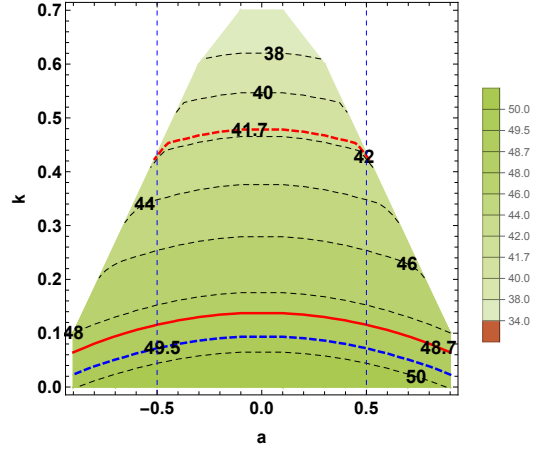
We note from Fig. 6 that in order to reproduce the central value of the angular diameter of the shadow ($48.7 \mu\text{as}$), k as high as 0.1 is allowed (red solid line in Fig. 6a and Fig. 6b) if we consider the following combinations of mass and distance: (a) $M = (3.975 \pm 0.058 \pm 0.026) \times 10^6 M_\odot$ and $D = 7959 \pm 59 \pm 32$ pc, (b) $M = (3.951 \pm 0.047) \times 10^6 M_\odot$ and $D = 7935 \pm 50$ pc. When the mass and distance reported by the Gravity collaboration is used, k as high as 0.2 is allowed (from the red solid line in Fig. 6c and Fig. 6d). If we wish to reproduce the angular diameter of the shadow upto $1-\sigma$ (red dashed line Fig. 6) then all the four combinations of mass and distance allow k as high as 0.5 (Fig. 6). However, we do not emphasize much on this result as the error bar of ± 7 associated with the shadow diameter is quite high. Therefore, when shadow diameter is considered a small but non-trivial value of k explains the observation better than the Kerr scenario.

However, when the image diameter is considered k as high as 0.05 is allowed within $1-\sigma$ (blue dashed line in Fig. 6a and Fig. 6b) if we assume mass and distance measurements by the Keck collaboration. Therefore, the Kerr scenario can reproduce the image diameter better in this case. When the mass and distance reported by the Gravity collaboration is used to calculate the angular diameter, then a small but non-trivial $k \simeq 0.05$ can reproduce the central value of $51.8 \mu\text{as}$ (blue solid line in Fig. 6c and Fig. 6d) while $k \simeq 0.15$ is allowed within $1-\sigma$ (blue dashed line in Fig. 6c and Fig. 6d). Hence, in this case the regular black hole scenario is more favored compared to the Kerr scenario.

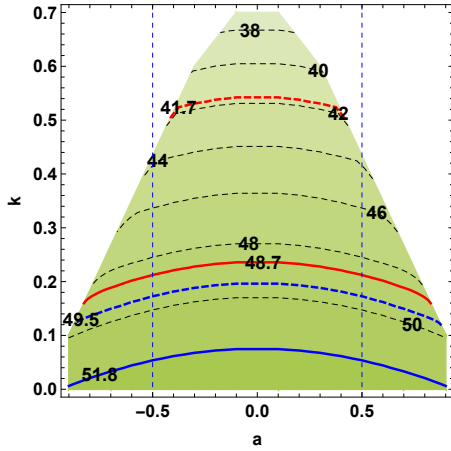
From the above discussion we note that the present observation related to the shadow of Sgr A* generally favors a small value of the non-linear electrodynamics charge parameter k . We also plot the variation of the axis ratio ΔA and the deviation from circularity ΔC for the shadow of Sgr A* as function of k and a . This is illustrated in Fig. 7. At present we do not have constraints on ΔA and ΔC from the shadow of Sgr A*. In future when these are reported we can establish independent constraints on k and a , just as we did for M87*.



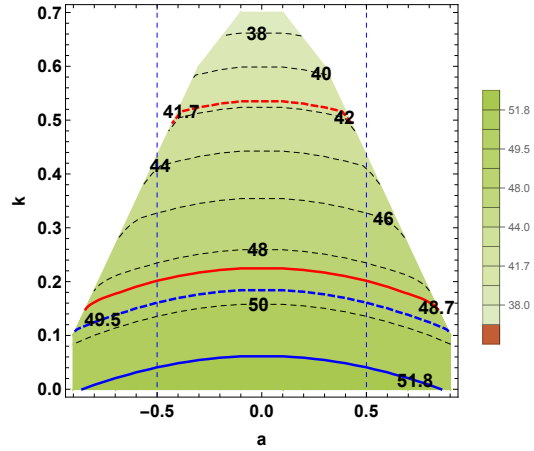
(a) The above figure depicts the angular diameter in the $k - a$ plane assuming $M = 3.951 \times 10^6 M_\odot$ and $D = 7.935$ kpc.



(b) The above figure depicts the angular diameter in the $k - a$ plane assuming $M = 3.975 \times 10^6 M_\odot$ and $D = 7.959$ kpc.

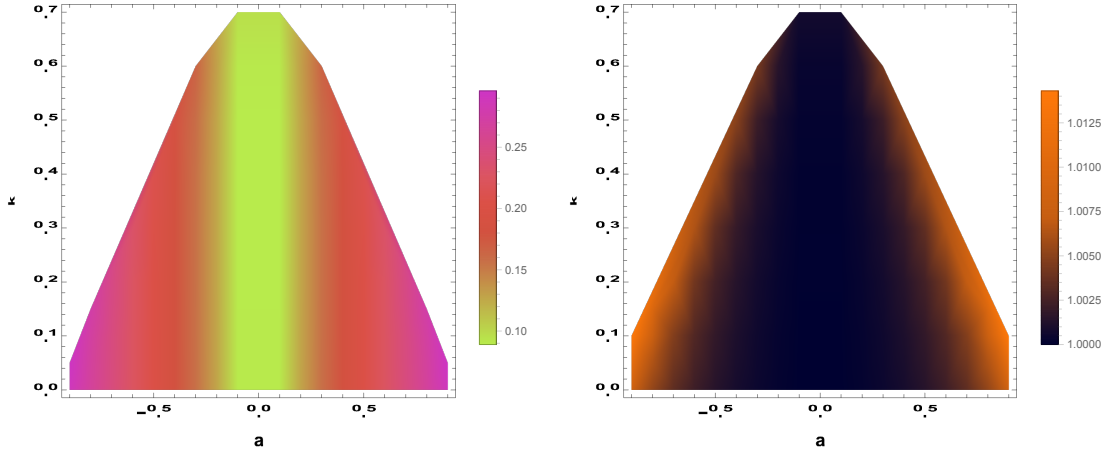


(c) The above figure depicts the angular diameter in the $k - a$ plane assuming $M = 4.261 \times 10^6 M_\odot$ and $D = 8.2467$ kpc.



(d) The above figure depicts the angular diameter in the $k - a$ plane assuming $M = 4.297 \times 10^6 M_\odot$ and $D = 8.277$ kpc.

Figure 6: The above figure shows the variation of the angular diameter of Sgr A* as function of k and a using masses and distances reported by the Keck team and the Gravity collaboration. In all cases the inclination angle is taken to be $i = 134^\circ$.



(a) The above figure shows the variation of ΔC with k and a assuming an inclination angle of 134° corresponding to Sgr A*.

(b) The above figure shows the variation of ΔA with k and a assuming an inclination angle of 134° corresponding to Sgr A*.

Figure 7: In the figure above we plot the variation of ΔC and ΔA as function of k and a , for the source Sgr A*. The inclination angle is taken to be 134° to obtain the plots.

5 Concluding Remarks

The present work investigates the role of the non-linear electrodynamic charge in explaining the recently observed shadow of M87* and Sgr A*. Such a charge arises in Einstein gravity coupled to non-linear electrodynamic and can potentially evade the $r = 0$ curvature singularity, which inevitably arises in GR. Such regular black holes are endowed with a de Sitter or a Minkowski core. The theoretical implications and observational consequences of regular black holes with a de Sitter core have been extensively studied in the past. This motivates us to explore the observational signatures of regular black holes with a Minkowski core. Such black holes have an exponential mass function which makes the corresponding quantum gravity theory finite to all orders.

We work out the nature of the black hole shadow for a general stationary and axisymmetric metric and subsequently specialize to the regular black hole scenario with a Minkowski core. Presence of an event horizon demands that the non-linear electrodynamic charge parameter k varies in the range $0 \lesssim k \lesssim 0.7$. Our study reveals that with increase in k the shadow becomes smaller in size. Non-rotating black holes and black holes viewed at 0° inclination angle cast a circular shadow. Deviation from circular shape occurs with increase in black hole spin or the inclination angle. This enables us to define a major axis ($\Delta\beta$) and a minor axis ($\Delta\alpha$) for the shadow which depends on the metric parameters k and a .

Derivation of the theoretical outline of the shadow enables us to compute the shadow related observables, namely, the angular diameter, the deviation from circularity and the axis ratio which are subsequently compared with the observed shadow of M87* and Sgr A*. Computation of the angular diameter requires one to provide information regarding the mass and the distance, e.g. an increase in mass enhances the shadow angular diameter. Thus, it turns out that for M87* when $M = 3.5 \times 10^9 M_\odot$ (obtained from gas dynamics measurements) is used to calculate the theoretical angular diameter, it cannot reproduce the

observed angular diameter of $42 \pm 3 \mu\text{as}$. Even when the mass of M87* based on stellar dynamics observation is used (i.e. $M = 6.2 \times 10^9 M_\odot$, which is considerably larger than the previous one) the observed angular diameter of the shadow cannot be reproduced. However, if one considers the maximum offset of 10% in the shadow diameter then $0.05 \lesssim k \lesssim 0.15$ can reproduce the observed angular diameter within $1-\sigma$. Therefore, the shadow of M87* can be explained by the regular black hole scenario with a small but non-zero value of k . It is interesting to note that the shadow angular diameter scales with the mass of the black hole. This might be the plausible reason the mass of M87* derived from the observed angular diameter (of $42 \pm 3 \mu\text{as}$) is $6.5 \times 10^9 M_\odot$ which is greater than both the previous estimates.

Mass and distance of Sgr A* have been well constrained by the Keck team and the Gravity collaboration. When mass and distance reported by the Keck team is used to compute the theoretical angular diameter, we note that $0.05 \lesssim k \lesssim 0.1$ best explains the central value of the observed shadow angular diameter. Again when mass and distance reported by the Gravity collaboration is used to evaluate the theoretical angular diameter, $0.15 \lesssim k \lesssim 0.2$ is required to address the observation of $48.7 \mu\text{as}$. Therefore, for the case of Sgr A* the regular black hole scenario is more favored compared to the Kerr scenario. In particular, a small but non-trivial value of k is required to reproduce the observed angular diameter of Sgr A*.

It is interesting to note that the present results are consistent with our previous works where we established constraints on k from observations associated with QPOs [61] and the continuum spectrum [112]. From the QPO related observations we found that some QPO models favor the Kerr scenario while most of them indicate that a small value of k explains the observations better. The optical observations of quasars on the other hand exhibit preference towards the Kerr scenario. It is important to note that none of the observations (shadow, QPO or continuum spectrum) favor a high value of k . This is interesting as these works are based on completely different observational samples and they collectively indicate towards the same finding. This outcome can be subjected to further test with the availability of more and more images of black holes with increasingly better resolution.

Acknowledgements

The research of SSG is partially supported by the Science and Engineering Research Board-Extra Mural Research Grant No. (EMR/2017/001372), Government of India. Research of I.B. is funded by the Start-Up Research Grant from SERB, DST, Government of India (Reg. No. SRG/2021/000418).

References

- [1] **LIGO Scientific, Virgo** Collaboration, B. P. Abbott *et al.*, “Observation of Gravitational Waves from a Binary Black Hole Merger,” *Phys. Rev. Lett.* **116** no. 6, (2016) 061102, [arXiv:1602.03837 \[gr-qc\]](#).
- [2] **LIGO Scientific, Virgo** Collaboration, B. P. Abbott *et al.*, “GW170817: Observation of Gravitational Waves from a Binary Neutron Star Inspiral,” *Phys. Rev. Lett.* **119** no. 16, (2017) 161101, [arXiv:1710.05832 \[gr-qc\]](#).
- [3] **Event Horizon Telescope** Collaboration, V. L. Fish, K. Akiyama, K. L. Bouman, A. A. Chael, M. D. Johnson, S. S. Doleman, L. Blackburn, J. F. C. Wardle, and W. T. Freeman, “Observing—and Imaging—Active Galactic Nuclei with the Event Horizon Telescope,” *Galaxies* **4** no. 4, (2016) 54, [arXiv:1607.03034 \[astro-ph.IM\]](#).

- [4] **Event Horizon Telescope** Collaboration, K. Akiyama *et al.*, “First M87 Event Horizon Telescope Results. I. The Shadow of the Supermassive Black Hole,” *Astrophys. J.* **875** no. 1, (2019) L1, [arXiv:1906.11238](#) [[astro-ph.GA](#)].
- [5] **Event Horizon Telescope** Collaboration, K. Akiyama *et al.*, “First M87 Event Horizon Telescope Results. II. Array and Instrumentation,” *Astrophys. J.* **875** no. 1, (2019) L2, [arXiv:1906.11239](#) [[astro-ph.IM](#)].
- [6] **Event Horizon Telescope** Collaboration, K. Akiyama *et al.*, “First M87 Event Horizon Telescope Results. III. Data Processing and Calibration,” *Astrophys. J.* **875** no. 1, (2019) L3, [arXiv:1906.11240](#) [[astro-ph.GA](#)].
- [7] **Event Horizon Telescope** Collaboration, K. Akiyama *et al.*, “First M87 Event Horizon Telescope Results. IV. Imaging the Central Supermassive Black Hole,” *Astrophys. J.* **875** no. 1, (2019) L4, [arXiv:1906.11241](#) [[astro-ph.GA](#)].
- [8] **Event Horizon Telescope** Collaboration, K. Akiyama *et al.*, “First M87 Event Horizon Telescope Results. V. Physical Origin of the Asymmetric Ring,” *Astrophys. J.* **875** no. 1, (2019) L5, [arXiv:1906.11242](#) [[astro-ph.GA](#)].
- [9] **Event Horizon Telescope** Collaboration, K. Akiyama *et al.*, “First M87 Event Horizon Telescope Results. VI. The Shadow and Mass of the Central Black Hole,” *Astrophys. J.* **875** no. 1, (2019) L6, [arXiv:1906.11243](#) [[astro-ph.GA](#)].
- [10] M. Milgrom, “A Modification of the Newtonian dynamics: Implications for galaxies,” *Astrophys. J.* **270** (1983) 371–383.
- [11] J. Bekenstein and M. Milgrom, “Does the missing mass problem signal the breakdown of Newtonian gravity?,” *Astrophys. J.* **286** (1984) 7–14.
- [12] **Supernova Cosmology Project** Collaboration, S. Perlmutter *et al.*, “Measurements of Omega and Lambda from 42 high redshift supernovae,” *Astrophys. J.* **517** (1999) 565–586, [arXiv:astro-ph/9812133](#) [[astro-ph](#)].
- [13] **Supernova Search Team** Collaboration, A. G. Riess *et al.*, “Observational evidence from supernovae for an accelerating universe and a cosmological constant,” *Astron. J.* **116** (1998) 1009–1038, [arXiv:astro-ph/9805201](#) [[astro-ph](#)].
- [14] R. Penrose, “Gravitational collapse and space-time singularities,” *Phys. Rev. Lett.* **14** (1965) 57–59.
- [15] S. W. Hawking, “Breakdown of Predictability in Gravitational Collapse,” *Phys. Rev.* **D14** (1976) 2460–2473.
- [16] D. Christodoulou, “The formation of black holes and singularities in spherically symmetric gravitational collapse,” *Commun. Pure Appl. Math.* **44** no. 3, (1991) 339–373.
- [17] S. W. Hawking and G. F. R. Ellis, *The Large Scale Structure of Space-Time*. Cambridge Monographs on Mathematical Physics. Cambridge University Press, 2, 2011.
- [18] P. Horava and E. Witten, “Heterotic and type I string dynamics from eleven-dimensions,” *Nucl.Phys.* **B460** (1996) 506–524, [arXiv:hep-th/9510209](#) [[hep-th](#)].

- [19] P. Horava and E. Witten, “Eleven-dimensional supergravity on a manifold with boundary,” *Nucl.Phys.* **B475** (1996) 94–114, [arXiv:hep-th/9603142 \[hep-th\]](#).
- [20] J. Polchinski, “String theory. Vol. 1: An introduction to the bosonic string,”.
- [21] J. Polchinski, “String theory. Vol. 2: Superstring theory and beyond,”.
- [22] A. Ashtekar, T. Pawłowski, and P. Singh, “Quantum nature of the big bang,” *Phys. Rev. Lett.* **96** (2006) 141301, [arXiv:gr-qc/0602086 \[gr-qc\]](#).
- [23] D. Kothawala, “Minimal Length and Small Scale Structure of Spacetime,” *Phys. Rev.* **D88** no. 10, (2013) 104029, [arXiv:1307.5618 \[gr-qc\]](#).
- [24] E. Ayon-Beato and A. Garcia, “The Bardeen model as a nonlinear magnetic monopole,” *Phys. Lett. B* **493** (2000) 149–152, [arXiv:gr-qc/0009077](#).
- [25] E. Ayon-Beato and A. Garcia, “Regular black hole in general relativity coupled to nonlinear electrodynamics,” *Phys. Rev. Lett.* **80** (1998) 5056–5059, [arXiv:gr-qc/9911046](#).
- [26] E. Ayon-Beato and A. Garcia, “Four parametric regular black hole solution,” *Gen. Rel. Grav.* **37** (2005) 635, [arXiv:hep-th/0403229](#).
- [27] K. A. Bronnikov, “Regular magnetic black holes and monopoles from nonlinear electrodynamics,” *Phys. Rev. D* **63** (2001) 044005, [arXiv:gr-qc/0006014](#).
- [28] A. Borde, “Regular black holes and topology change,” *Phys. Rev. D* **55** (1997) 7615–7617, [arXiv:gr-qc/9612057](#).
- [29] C. Barrabes and V. P. Frolov, “How many new worlds are inside a black hole?,” *Phys. Rev. D* **53** (1996) 3215–3223, [arXiv:hep-th/9511136](#).
- [30] E. Ayon-Beato and A. Garcia, “Nonsingular charged black hole solution for nonlinear source,” *Gen. Rel. Grav.* **31** (1999) 629–633, [arXiv:gr-qc/9911084](#).
- [31] A. Bonanno and M. Reuter, “Renormalization group improved black hole space-times,” *Phys. Rev. D* **62** (2000) 043008, [arXiv:hep-th/0002196](#).
- [32] P. Nicolini, A. Smailagic, and E. Spallucci, “Noncommutative geometry inspired Schwarzschild black hole,” *Phys. Lett. B* **632** (2006) 547–551, [arXiv:gr-qc/0510112](#).
- [33] Y. S. Myung, Y.-W. Kim, and Y.-J. Park, “Quantum Cooling Evaporation Process in Regular Black Holes,” *Phys. Lett. B* **656** (2007) 221–225, [arXiv:gr-qc/0702145](#).
- [34] S. A. Hayward, “Formation and evaporation of nonsingular black holes,” *Phys. Rev. Lett.* **96** (Jan, 2006) 031103. <https://link.aps.org/doi/10.1103/PhysRevLett.96.031103>.
- [35] V. P. Frolov, M. A. Markov, and V. F. Mukhanov, “Black Holes as Possible Sources of Closed and Semiclosed Worlds,” *Phys. Rev. D* **41** (1990) 383.
- [36] V. F. Mukhanov and R. H. Brandenberger, “A Nonsingular universe,” *Phys. Rev. Lett.* **68** (1992) 1969–1972.

- [37] R. H. Brandenberger, V. F. Mukhanov, and A. Sornborger, “A Cosmological theory without singularities,” *Phys. Rev. D* **48** (1993) 1629–1642, [arXiv:gr-qc/9303001](#).
- [38] S. Ansoldi, “Spherical black holes with regular center: A Review of existing models including a recent realization with Gaussian sources,” in *Conference on Black Holes and Naked Singularities*, 2, 2008. [arXiv:0802.0330 \[gr-qc\]](#).
- [39] E. B. Gliner, “Algebraic Properties of the Energy-momentum Tensor and Vacuum-like States of Matter,” *Soviet Journal of Experimental and Theoretical Physics* **22** (Feb., 1966) 378.
- [40] Z.-Y. Fan and X. Wang, “Construction of Regular Black Holes in General Relativity,” *Phys. Rev. D* **94** no. 12, (2016) 124027, [arXiv:1610.02636 \[gr-qc\]](#).
- [41] H. Culetu, “On a regular charged black hole with a nonlinear electric source,” *Int. J. Theor. Phys.* **54** no. 8, (2015) 2855–2863, [arXiv:1408.3334 \[gr-qc\]](#).
- [42] M. R. Brown, “Is Quantum Gravity Finite?,” in *Oxford Conference on Quantum Gravity*. 1980.
- [43] J. W. Moffat, “Quantum gravity resolution to the cosmological constant problem,” [arXiv:hep-ph/0102088](#).
- [44] E. T. Newman and A. I. Janis, “Note on the Kerr spinning particle metric,” *J. Math. Phys.* **6** (1965) 915–917.
- [45] M. Azreg-Aïnou, “Generating rotating regular black hole solutions without complexification,” *Phys. Rev. D* **90** no. 6, (2014) 064041, [arXiv:1405.2569 \[gr-qc\]](#).
- [46] M. Azreg-Aïnou, “From static to rotating to conformal static solutions: Rotating imperfect fluid wormholes with(out) electric or magnetic field,” *Eur. Phys. J. C* **74** no. 5, (2014) 2865, [arXiv:1401.4292 \[gr-qc\]](#).
- [47] M. Azreg-Aïnou, “Regular and conformal regular cores for static and rotating solutions,” *Phys. Lett. B* **730** (2014) 95–98, [arXiv:1401.0787 \[gr-qc\]](#).
- [48] S. G. Ghosh, “A nonsingular rotating black hole,” *Eur. Phys. J. C* **75** no. 11, (2015) 532, [arXiv:1408.5668 \[gr-qc\]](#).
- [49] R. Kumar and S. G. Ghosh, “Photon ring structure of rotating regular black holes and no-horizon spacetimes,” *Class. Quant. Grav.* **38** no. 8, (2021) 8, [arXiv:2004.07501 \[gr-qc\]](#).
- [50] R. Kumar, A. Kumar, and S. G. Ghosh, “Testing Rotating Regular Metrics as Candidates for Astrophysical Black Holes,” *Astrophys. J.* **896** no. 1, (2020) 89, [arXiv:2006.09869 \[gr-qc\]](#).
- [51] A. Allahyari, M. Khodadi, S. Vagnozzi, and D. F. Mota, “Magnetically charged black holes from non-linear electrodynamics and the Event Horizon Telescope,” *JCAP* **02** (2020) 003, [arXiv:1912.08231 \[gr-qc\]](#).
- [52] S. Vagnozzi, R. Roy, Y.-D. Tsai, and L. Visinelli, “Horizon-scale tests of gravity theories and fundamental physics from the Event Horizon Telescope image of Sagittarius A*,” [arXiv:2205.07787 \[gr-qc\]](#).

- [53] A. Uniyal, R. C. Pantig, and A. Övgün, “Probing a nonlinear electrodynamics black hole with thin accretion disk, shadow and deflection angle with M87* and Sgr A* from EHT,” [arXiv:2205.11072 \[gr-qc\]](#).
- [54] Z. Stuchlík and J. Schee, “Circular geodesic of Bardeen and Ayon–Beato–Garcia regular black-hole and no-horizon spacetimes,” *Int. J. Mod. Phys. D* **24** no. 02, (2014) 1550020, [arXiv:1501.00015 \[astro-ph.HE\]](#).
- [55] J. Schee and Z. Stuchlík, “Gravitational lensing and ghost images in the regular Bardeen no-horizon spacetimes,” *JCAP* **06** (2015) 048, [arXiv:1501.00835 \[astro-ph.HE\]](#).
- [56] J. Schee and Z. Stuchlík, “Profiled spectral lines generated by Keplerian discs orbiting in the Bardeen and Ayon–Beato–Garcia spacetimes,” *Class. Quant. Grav.* **33** no. 8, (2016) 085004, [arXiv:1604.00632 \[gr-qc\]](#).
- [57] Z. Stuchlík and J. Schee, “Shadow of the regular Bardeen black holes and comparison of the motion of photons and neutrinos,” *Eur. Phys. J. C* **79** no. 1, (2019) 44.
- [58] J. Schee and Z. Stuchlík, “Profiled spectral lines of Keplerian rings orbiting in the regular Bardeen black hole spacetimes,” *Eur. Phys. J. C* **79** no. 12, (2019) 988, [arXiv:1908.07197 \[gr-qc\]](#).
- [59] I. Banerjee, “Deciphering signatures of Bardeen black holes from the observed quasi-periodic oscillations,” *JCAP* **05** no. 05, (2022) 020, [arXiv:2201.00679 \[gr-qc\]](#).
- [60] I. Banerjee, V. S. Chawan, B. Mandal, S. K. Sahoo, and S. SenGupta, “Quasar continuum spectrum disfavors black holes with a magnetic monopole charge,” *Phys. Rev. D* **105** no. 6, (2022) 064073, [arXiv:2112.05385 \[gr-qc\]](#).
- [61] I. Banerjee, “Testing black holes in non-linear electrodynamics from the observed quasi-periodic oscillations,” [arXiv:2203.10890 \[gr-qc\]](#).
- [62] **Event Horizon Telescope** Collaboration, K. Akiyama *et al.*, “First Sagittarius A* Event Horizon Telescope Results. I. The Shadow of the Supermassive Black Hole in the Center of the Milky Way,” *Astrophys. J. Lett.* **930** no. 2, (2022) L12.
- [63] **Event Horizon Telescope** Collaboration, K. Akiyama *et al.*, “First Sagittarius A* Event Horizon Telescope Results. II. EHT and Multiwavelength Observations, Data Processing, and Calibration,” *Astrophys. J. Lett.* **930** no. 2, (2022) L13.
- [64] **Event Horizon Telescope** Collaboration, K. Akiyama *et al.*, “First Sagittarius A* Event Horizon Telescope Results. III. Imaging of the Galactic Center Supermassive Black Hole,” *Astrophys. J. Lett.* **930** no. 2, (2022) L14.
- [65] **Event Horizon Telescope** Collaboration, K. Akiyama *et al.*, “First Sagittarius A* Event Horizon Telescope Results. IV. Variability, Morphology, and Black Hole Mass,” *Astrophys. J. Lett.* **930** no. 2, (2022) L15.
- [66] **Event Horizon Telescope** Collaboration, K. Akiyama *et al.*, “First Sagittarius A* Event Horizon Telescope Results. V. Testing Astrophysical Models of the Galactic Center Black Hole,” *Astrophys. J. Lett.* **930** no. 2, (2022) L16.

- [67] **Event Horizon Telescope** Collaboration, K. Akiyama *et al.*, “First Sagittarius A* Event Horizon Telescope Results. VI. Testing the Black Hole Metric,” *Astrophys. J. Lett.* **930** no. 2, (2022) L17.
- [68] I. H. Salazar, A. Garcia, and J. Plebanski, “Duality Rotations and Type D Solutions to Einstein Equations With Nonlinear Electromagnetic Sources,” *J. Math. Phys.* **28** (1987) 2171–2181.
- [69] K. A. Bronnikov, “Comment on “Construction of regular black holes in general relativity”,” *Phys. Rev. D* **96** no. 12, (2017) 128501, [arXiv:1712.04342 \[gr-qc\]](#).
- [70] B. Toshmatov, Z. Stuchlík, and B. Ahmedov, “Comment on “Construction of regular black holes in general relativity”,” *Phys. Rev. D* **98** no. 2, (2018) 028501, [arXiv:1807.09502 \[gr-qc\]](#).
- [71] J. M. Bardeen, “Non-singular general-relativistic gravitational collapse,” in *Proceedings of the International Conference GR5, Tiflis U.S.S.R.* 1968.
- [72] I. Dymnikova, “Vacuum nonsingular black hole,” *Gen. Rel. Grav.* **24** (1992) 235–242.
- [73] I. Dymnikova, “Regular electrically charged structures in nonlinear electrodynamics coupled to general relativity,” *Class. Quant. Grav.* **21** (2004) 4417–4429, [arXiv:gr-qc/0407072](#).
- [74] K. A. Bronnikov and J. C. Fabris, “Regular phantom black holes,” *Phys. Rev. Lett.* **96** (2006) 251101, [arXiv:gr-qc/0511109](#).
- [75] A. Burinskii and S. R. Hildebrandt, “New type of regular black holes and particle - like solutions from NED,” *Phys. Rev. D* **65** (2002) 104017, [arXiv:hep-th/0202066](#).
- [76] W. Berej, J. Matyjasek, D. Tryniecki, and M. Woronowicz, “Regular black holes in quadratic gravity,” *Gen. Rel. Grav.* **38** (2006) 885–906, [arXiv:hep-th/0606185](#).
- [77] L. Balart and E. C. Vagenas, “Regular black holes with a nonlinear electrodynamics source,” *Phys. Rev. D* **90** no. 12, (2014) 124045, [arXiv:1408.0306 \[gr-qc\]](#).
- [78] S. N. Sajadi and N. Riazi, “Nonlinear electrodynamics and regular black holes,” *Gen. Rel. Grav.* **49** no. 3, (2017) 45. [Erratum: *Gen.Rel.Grav.* 52, 18 (2020)].
- [79] S. G. Ghosh, D. V. Singh, and S. D. Maharaj, “Regular black holes in Einstein-Gauss-Bonnet gravity,” *Phys. Rev. D* **97** no. 10, (2018) 104050.
- [80] E. Ayon-Beato and A. Garcia, “New regular black hole solution from nonlinear electrodynamics,” *Phys. Lett. B* **464** (1999) 25, [arXiv:hep-th/9911174](#).
- [81] H. Culetu, “On a regular modified Schwarzschild spacetime,” [arXiv:1305.5964 \[gr-qc\]](#).
- [82] S. R. Valluri, D. J. Jeffrey, and R. M. Corless, “Some applications of the Lambert W function to physics,” *Can. J. Phys.* **78** (2000) 823–831.
- [83] P. Boonserm and M. Visser, “Bounding the greybody factors for Schwarzschild black holes,” *Phys. Rev. D* **78** (2008) 101502, [arXiv:0806.2209 \[gr-qc\]](#).
- [84] P. Boonserm and M. Visser, “Quasi-normal frequencies: Key analytic results,” *JHEP* **03** (2011) 073, [arXiv:1005.4483 \[math-ph\]](#).

- [85] P. Boonserm, T. Ngampitipan, and M. Visser, “Regge-Wheeler equation, linear stability, and greybody factors for dirty black holes,” *Phys. Rev. D* **88** (2013) 041502, [arXiv:1305.1416 \[gr-qc\]](#).
- [86] P. Boonserm, T. Ngampitipan, A. Simpson, and M. Visser, “Exponential metric represents a traversable wormhole,” *Phys. Rev. D* **98** no. 8, (2018) 084048, [arXiv:1805.03781 \[gr-qc\]](#).
- [87] H. Sonoda, “Solving renormalization group equations with the Lambert W function,” *Phys. Rev. D* **87** no. 8, (2013) 085023, [arXiv:1302.6069 \[hep-th\]](#).
- [88] H. Sonoda, “Analytic form of the effective potential in the large N limit of a real scalar theory in four dimensions,” [arXiv:1302.6059 \[hep-th\]](#).
- [89] S. E. Gralla, D. E. Holz, and R. M. Wald, “Black Hole Shadows, Photon Rings, and Lensing Rings,” *Phys. Rev. D* **100** no. 2, (2019) 024018, [arXiv:1906.00873 \[astro-ph.HE\]](#).
- [90] C. Bambi, K. Freese, S. Vagnozzi, and L. Visinelli, “Testing the rotational nature of the supermassive object M87* from the circularity and size of its first image,” *Phys. Rev. D* **100** no. 4, (2019) 044057, [arXiv:1904.12983 \[gr-qc\]](#).
- [91] K. Hioki and K.-i. Maeda, “Measurement of the Kerr Spin Parameter by Observation of a Compact Object’s Shadow,” *Phys. Rev. D* **80** (2009) 024042, [arXiv:0904.3575 \[astro-ph.HE\]](#).
- [92] S. Vagnozzi and L. Visinelli, “Hunting for extra dimensions in the shadow of M87*,” *Phys. Rev. D* **100** no. 2, (2019) 024020, [arXiv:1905.12421 \[gr-qc\]](#).
- [93] I. Banerjee, S. Chakraborty, and S. SenGupta, “Silhouette of M87*: A New Window to Peek into the World of Hidden Dimensions,” *Phys. Rev. D* **101** no. 4, (2020) 041301, [arXiv:1909.09385 \[gr-qc\]](#).
- [94] P. V. P. Cunha and C. A. R. Herdeiro, “Shadows and strong gravitational lensing: a brief review,” *Gen. Rel. Grav.* **50** no. 4, (2018) 42, [arXiv:1801.00860 \[gr-qc\]](#).
- [95] A. de Vries, “The apparent shape of a rotating charged black hole, closed photon orbits and the bifurcation set A_4 ,” *Classical and Quantum Gravity* **17** no. 1, (Dec, 1999) 123–144. <https://doi.org/10.1088%2F0264-9381%2F17%2F1%2F309>.
- [96] Z. Stuchlík, M. Kološ, J. Kovář, P. Slaný, and A. Tursunov, “Influence of Cosmic Repulsion and Magnetic Fields on Accretion Disks Rotating around Kerr Black Holes,” *Universe* **6** no. 2, (2020) 26.
- [97] Y. Zhang and P. M. Bellan, “Neutral-charged-particle collisions as the mechanism for accretion disk angular momentum transport,” *The Astrophysical Journal* **930** no. 2, (May, 2022) 167. <https://doi.org/10.3847/1538-4357/ac62d5>.
- [98] E. Teo, “Spherical Photon Orbits Around a Kerr Black Hole,” *General Relativity and Gravitation* **35** no. 11, (Nov., 2003) 1909–1926.
- [99] J. M. Bardeen, “Timelike and null geodesics in the Kerr metric,” in *Proceedings, Ecole d’Eté de Physique Théorique: Les Astres Occlus: Les Houches, France, August, 1972*, pp. 215–240. 1973.

- [100] B. Carter, “Global structure of the Kerr family of gravitational fields,” *Phys. Rev.* **174** (1968) 1559–1571.
- [101] C. T. Cunningham and J. M. Bardeen, “The Optical Appearance of a Star Orbiting an Extreme Kerr Black Hole,” *Apj* **183** (July, 1973) 237–264.
- [102] A. de Vries, “The apparent shape of a rotating charged black hole, closed photon orbits and the bifurcation set A_4 ,” *Classical and Quantum Gravity* **17** no. 1, (Jan., 2000) 123–144.
- [103] N. Tsukamoto, Z. Li, and C. Bambi, “Constraining the spin and the deformation parameters from the black hole shadow,” *JCAP* **06** (2014) 043, [arXiv:1403.0371 \[gr-qc\]](#).
- [104] M. Amir and S. G. Ghosh, “Shapes of rotating nonsingular black hole shadows,” *Phys. Rev. D* **94** no. 2, (2016) 024054, [arXiv:1603.06382 \[gr-qc\]](#).
- [105] N. Tsukamoto, “Black hole shadow in an asymptotically-flat, stationary, and axisymmetric spacetime: The Kerr-Newman and rotating regular black holes,” *Phys. Rev. D* **97** no. 6, (2018) 064021, [arXiv:1708.07427 \[gr-qc\]](#).
- [106] K. Gebhardt, J. Adams, D. Richstone, T. R. Lauer, S. M. Faber, K. Gultekin, J. Murphy, and S. Tremaine, “The Black-Hole Mass in M87 from Gemini/NIFS Adaptive Optics Observations,” *Astrophys. J.* **729** (2011) 119, [arXiv:1101.1954 \[astro-ph.CO\]](#).
- [107] J. L. Walsh, A. J. Barth, L. C. Ho, and M. Sarzi, “The M87 Black Hole Mass from Gas-dynamical Models of Space Telescope Imaging Spectrograph Observations,” *Astrophys. J.* **770** (2013) 86, [arXiv:1304.7273 \[astro-ph.CO\]](#).
- [108] J. P. Blakeslee, A. Jordan, S. Mei, P. Cote, L. Ferrarese, L. Infante, E. W. Peng, J. L. Tonry, and M. J. West, “The ACS Fornax Cluster Survey. V. Measurement and Recalibration of Surface Brightness Fluctuations and a Precise Value of the Fornax–Virgo Relative Distance,” *Astrophys. J.* **694** (2009) 556–572, [arXiv:0901.1138 \[astro-ph.CO\]](#).
- [109] S. Bird, W. E. Harris, J. P. Blakeslee, and C. Flynn, “The Inner Halo of M87: A First Direct View of the Red-Giant Population,” *Astron. Astrophys.* **524** (2010) A71, [arXiv:1009.3202 \[astro-ph.GA\]](#).
- [110] M. Cantiello *et al.*, “A Precise Distance to the Host Galaxy of the Binary Neutron Star Merger GW170817 Using Surface Brightness Fluctuations,” *Astrophys. J.* **854** no. 2, (2018) L31, [arXiv:1801.06080 \[astro-ph.GA\]](#).
- [111] Török, G., Abramowicz, M. A., Kluźniak, W., and Stuchlík, Z., “The orbital resonance model for twin peak khz quasi periodic oscillations in microquasars,” *A&A* **436** no. 1, (2005) 1–8. <https://doi.org/10.1051/0004-6361:20047115>.
- [112] I. Banerjee, “Signatures of regular black holes from the quasar continuum spectrum,” [arXiv:2206.06899 \[gr-qc\]](#).